Evolution of Dark Energy Reconstructed from the Latest Observations

Yuting Wang[1] , Levon Pogosian[2,3], Gong-Bo Zhao[1,3,4] , and Alex Zucca[2]

[1] National Astronomy Observatories, Chinese Academy of Science, Beijing, 100101, People's Republic of China; ytwang@nao.cas.cn
[2] Department of Physics, Simon Fraser University, Burnaby, British Columbia, V5A 1S6, Canada
[3] Institute of Cosmology and Gravitation, University of Portsmouth, Portsmouth PO1 3FX, UK
[4] University of Chinese Academy of Sciences, Beijing, 100049, People's Republic of China

Abstract

We reconstruct the evolution of the dark energy (DE) density using a nonparametric Bayesian approach from a combination of the latest observational data. We caution against parameterizing DE in terms of its equation of state as it can be singular in modified gravity models, and using it introduces a bias preventing negative effective DE densities. We find a 3.7σ preference for an evolving effective DE density with interesting features. For example, it oscillates around the Λ cold dark matter prediction at $z \lesssim 0.7$, and could be negative at $z \gtrsim 2.3$; DE can be pressure-less at multiple redshifts, and a short period of cosmic deceleration is allowed at $0.1 \lesssim z \lesssim 0.2$. We perform the reconstruction for several choices of the prior, as well as a evidence-weighted reconstruction. We find that some of the dynamical features, such as the oscillatory behavior of the DE density, are supported by the Bayesian evidence, which is a first detection of a dynamical DE with a positive Bayesian evidence. The evidence-weighted reconstruction prefers a dynamical DE at a $(2.5 \pm 0.06)\sigma$ significance level.

Key words: dark energy

1. Introduction

Since becoming the working model of cosmology following the discovery of cosmic acceleration (Riess et al. 1998; Perlmutter et al. 1999), the Λ cold dark matter (ΛCDM) model has withstood all of the tests using increasingly accurate and comprehensive cosmic microwave background (CMB; Bennett et al. 2013; Planck Collaboration et al. 2016), supernovae (SNe; Conley et al. 2011; Suzuki et al. 2012), galaxy clustering (Zehavi et al. 2011), and weak lensing (Heymans et al. 2013; Hildebrandt et al. 2017) data. There are, however, good reasons to keep an open mind regarding possible extensions and alternatives to ΛCDM. The two main ingredients of the model, Λ and CDM, are not understood at a fundamental level. Direct searches of dark matter have so far failed, while the observed value of the vacuum energy implies a technically unnatural fine-tuning of Λ in the context of the effective field theory (Burgess 2017). This is the framework for the present understanding of particle interactions.

The recent exquisite measurements of the CMB temperature and polarization by *Planck* (Planck Collaboration et al. 2016) significantly reduced the uncertainties in ΛCDM parameters. With this dramatic improvement in precision, it is perhaps not surprising that several 2–3σ level tensions have appeared between *Planck* and other data sets, as well as within the *Planck* data itself (Addison et al. 2016), when interpreted within the ΛCDM model. For instance, the locally measured value of the Hubble constant H_0 is off by 3.5σ from the *Planck* best fit (Riess et al. 2016). The expansion rate at $z = 2.34$, implied by the Baryon Oscillation Spectroscopic Survey (BOSS) baryonic acoustic oscillations (BAOs) measurement from the Lyα forest (Font-Ribera et al. 2014; Delubac et al. 2015), disagrees with the best-fit ΛCDM prediction at a $\sim$2.7σ level. These tensions are not at a significance level sufficient to rule out ΛCDM—they could simply be statistical fluctuations (Scott 2018). It is also possible that they are caused by unaccounted systematic effects in the measurements, or the modeling of the data. However, it is worth noting that these tensions have persisted and become stronger over the past three years, fueling significant interest in possible extensions of ΛCDM, such as dynamical dark energy (DE; Di Valentino et al. 2017a; Solà et al. 2017; Zhao et al. 2017; Capozziello et al. 2018; Ooba et al. 2018; Solà Peracaula et al. 2018), interacting DE and dark matter (Das et al. 2006; Wang et al. 2015; Di Valentino et al. 2017b; Yang et al. 2018), and other extensions of ΛCDM.

A reconstruction of the effective DE equation of state (EOS) $w_{\mathrm{DE}}^{\mathrm{eff}}(a)$ from a combination of recent data was presented in Zhao et al. (2017), showing a clear preference for $w_{\mathrm{DE}}^{\mathrm{eff}} < -1$, along with a possible crossing of the $w_{\mathrm{DE}}^{\mathrm{eff}} = -1$ divide. Such behavior is impossible for quintessence—a minimally coupled scalar field with a canonical kinetic term (Ratra & Peebles 1988; Wetterich 1995, 2002; Caldwell et al. 1998; Steinhardt et al. 1999; Peebles & Ratra 2003), unless the sign of the kinetic term is changed by hand (Caldwell 2002; Carroll et al. 2003; Vikman 2005). This, however, leads to ghost instabilities, i.e., energy being unbounded from below, unless one postulates a non-Lorentz-invariant cutoff at an appropriately chosen scale (Cline et al. 2004). On the other hand, such "ghostly" behavior generically occurs in non-minimally coupled DE models, i.e., where DE and matter interact through an additional scalar force (Carroll et al. 2005; Das et al. 2006). There, the $w_{\mathrm{DE}}^{\mathrm{eff}}$ measured in Zhao et al. (2017) would not be the EOS of the scalar field, but it would be an effective quantity that depends on the coupling to matter. Such a $w_{\mathrm{DE}}^{\mathrm{eff}}$ is allowed to be phantom and to cross -1, with the effective DE density (defined below) allowed to change sign. In such cases, parameterizing the DE evolution via $w_{\mathrm{DE}}^{\mathrm{eff}}$ is unnecessarily restrictive as, by design, it does not allow for negative effective DE densities. To address this, we will directly reconstruct the effective DE density.

We define the effective DE in a purely phenomenological way, by letting it describe all of the contributions to the standard Friedmann equation other than matter and radiation. Namely, the effective DE density $\rho_{\mathrm{DE}}^{\mathrm{eff}}$ is defined via

$$\frac{H^2}{H_0^2} = \frac{\Omega_{\mathrm{r}}}{a^4} + \frac{\Omega_{\mathrm{M}}}{a^3} + \Omega_{\mathrm{DE}}X(a), \qquad (1)$$

where a is the scale factor, and $X(a) \equiv \rho_{\mathrm{DE}}^{\mathrm{eff}}(a)/\rho_{\mathrm{DE}}^{\mathrm{eff}}(1)$. $\rho_{\mathrm{DE}}^{\mathrm{eff}}$ could include modifications of gravity, non-minimal interactions with matter, etc. We assume a flat universe, so that $\Omega_{\mathrm{r}} + \Omega_{\mathrm{M}} + \Omega_{\mathrm{DE}} = 1$ and $H(a = 1) = H_0$.

Most studies of DE dynamics (but not all, see, e.g., Wang & Tegmark 2004; Sahni & Starobinsky 2006; Sahni et al. 2014; Poulin et al. 2018) attempt to measure the DE EOS, $w_{\mathrm{DE}} = p_{\mathrm{DE}}/\rho_{\mathrm{DE}}$. If DE is a conserved fluid with $\rho_{\mathrm{DE}} > 0$, then specifying $w_{\mathrm{DE}}(a)$ fully determines the dynamics of DE. In such a case, one can replace p_{DE} with $w_{\mathrm{DE}}\rho_{\mathrm{DE}}$ in the conservation equation, $\dot{\rho}_{\mathrm{DE}} + 3H\rho_{\mathrm{DE}}(1 + w_{\mathrm{DE}}) = 0$, and solve it to find $\rho_{\mathrm{DE}}(a) = \rho_{\mathrm{DE}}(1)\exp\left[\int_a^1 da' 3(1 + w_{\mathrm{DE}}(a'))\big/a'\right]$. Working with the EOS provides a simple test of the ΛCDM as $w_\Lambda = -1$ independent of the value of Λ. However, in theories where the DE field mediates a force between matter particles, the effective DE EOS, $w_{\mathrm{DE}}^{\mathrm{eff}} \equiv p_{\mathrm{DE}}^{\mathrm{eff}}/\rho_{\mathrm{DE}}^{\mathrm{eff}}$, can become singular, because $\rho_{\mathrm{DE}}^{\mathrm{eff}}$ can change sign (see Appendix A for details; Horndeski 1974; Deffayet et al. 2009a, 2009b, 2011; Gleyzes et al. 2015). Thus, parameterizing the expansion history $w_{\mathrm{DE}}^{\mathrm{eff}}$ in cosmological codes used for model-independent tests of gravity, such as MGCAMB (Zhao et al. 2009; Hojjati et al. 2011), EFTCAMB (Hu et al. 2014; Raveri et al. 2014), and hiCLASS (Zumalacárregui et al. 2017), could lead to a bias, as it assumes $\rho_{\mathrm{DE}}^{\mathrm{eff}} > 0$ at all times. This is particularly relevant because the data indicate a preference for $w_{\mathrm{DE}} < -1$, which is prohibited for quintessence but can happen in modified gravity and brane-world models (Damour et al. 1990; Torres 2002; Chung et al. 2003; Faraoni 2003; Sahni & Shtanov 2003; Carroll et al. 2005; Das et al. 2006). For these reasons, looking directly at the evolution of DE density is more appropriate. Avoiding the assumption of a positive ρ_{DE} also allows one to constrain models such as "Everpresent Λ" (Ahmed et al. 2004; Ahmed & Sorkin 2013; Zwane et al. 2017), in which the observed cosmological "constant" fluctuates between positive and negative values.

2. Data and Method

In what follows, we use the correlated prior method of (Crittenden et al. 2012, 2009) to reconstruct the evolution of the DE density from the available data sets used to probe the background expansion. We start with a brief review of the data sets and the reconstruction method.

Our phenomenological definition of the effective DE (1) does not specify the underlying theory needed for calculating cosmological perturbations. To keep the analysis general, we only evaluate observables predicted by the Friedmann equation and consider data sets probing the background expansion history. They include the CMB distance information from *Planck* (Planck Collaboration et al. 2016),[5] the "Joint Light-curve Analysis" (JLA) supernovae (Betoule et al. 2014), BAO measurements from 6dF Galaxy Survey (6dFGS; Beutler et al. 2011), Sloan Digital Sky Survey (SDSS) data release (DR)7 Main Galaxy Sample (MGS; Ross et al. 2015), tomographic BOSS DR12 (TomoBAO; Wang et al. 2017), eBOSS DR14 quasar sample (DR14Q; Ata et al. 2018) and the Lyα forest (LyαFBAO) of BOSS DR11 quasars (Font-Ribera et al. 2014; Delubac et al. 2015), the local measurement of $H_0 = 73.24 \pm 1.74$ [km s^{-1} Mpc^{-1}] in Riess et al. (2016),

and the Observational Hubble parameter Data (OHD; Moresco et al. 2016).

To reconstruct $X(a)$, we parameterize it in terms of its values at N points in a. Namely, we have bins $X_i = X(a_i)$, $i = 1, \ldots, N$, with a_i distributed uniformly in the interval $a \in [1, 0.001]$. We take $N = 40$, which is large enough so that further increases do not affect the reconstruction results. If X_i were assumed to be independent, fitting them to data would yield large uncertainties, rendering the reconstruction useless. Moreover, treating the bins as completely independent is an unreasonably strong assumption as, in any specific theory, the effective DE density would be correlated at nearby points in a. Motivated by these considerations, we use the method of Crittenden et al. (2009, 2012) and introduce a prior that correlates the neighboring bins. Specifically, we take $X(a)$ to be a Gaussian random variable with a given correlation ξ between its values at a and a', i.e., $\xi(|a - a'|) \equiv \langle[X(a) - X^{\mathrm{fid}}(a)][X(a') - X^{\mathrm{fid}}(a')]\rangle$. Here, $X^{\mathrm{fid}}(a)$ is a reference fiducial model, and the correlation function ξ is chosen so that it is nonzero for $|a - a'|$ below a given "correlation length" a_c, and approaches zero at larger separations. We adopt the CPZ form (Crittenden et al. 2009, 2012) for the correlation, namely, $\xi(|a - a'|) = \xi(0)/[1 + (|a - a'|/a_c)^2]$, where $\xi(0)$ sets the strength of the prior. The latter can be related to the expected variance in the mean value of X as $\sigma_m^2 \simeq \pi\xi(0)a_c/(a_{\max} - a_{\min})$. In practice, we set σ_m and a_c, and derive the corresponding $\xi(0)$.

As our "standard" working prior we adopt $a_c = 0.06$ and $\sigma_m = 0.04$, which were the values used in Zhao et al. (2017) to reconstruct $w_{\mathrm{DE}}(a)$. Their physical meaning is, of course, different, as w_{DE} and X are related through an integral and, therefore, have different correlation properties. To better understand the impact of the prior, we have also performed reconstructions using different values of a_c and σ_m. We find that our standard prior is rather weak in the sense that decreasing a_c or increasing σ_m increases the uncertainties but does not change the shape of the reconstruction. We show results with a few stronger priors in Appendix B. As expected, in the limit of $a_c \to 1$ or $\sigma_m \to 0$ the reconstructed X becomes a constant.

Our binning scheme for X includes eight bins in the redshift range $3 < z < 1000$, between the redshift of the LyαFBAO measurement and the CMB last scattering surface. The reason for keeping these eight bins, even though there are no data points in that range, was to simplify the evaluation of the prior covariance that can be performed analytically for uniformly spaced bins. However, physically no information can be gained from having these additional degrees of freedom at $z > 3$. To check the role that they play in the reconstruction, we replaced them with a single bin for $z \in [3.85, 1000]$. The value of X in the wide bin was either fixed to 1, or allowed to vary freely, uncorrelated with the 32 lower redshift bins. As shown in Appendix B, the reconstruction of X in the range probed by observations, $z \in [0, 3]$, is largely unaffected by what is assumed at higher redshifts.

We use PolyChord[6] (Handley et al. 2015a, 2015b), a nested sampling plug-in for CosmoMC[7] (Lewis & Bridle 2002), which enables computation of the Bayesian evidence, to sample the parameter space $\boldsymbol{P} = \{\Omega_b h^2, \Omega_c h^2, \Theta_s, X_i, \mathcal{N}\}$, where $\Omega_b h^2$ and $\Omega_c h^2$ are the physical densities of baryon

---

and CDM, respectively, Θ_s is the ratio of the sound horizon to the angular diameter distance at the decoupling epoch (multiplied by 100), X_i ($i = 1, ..., 40$) are the binned DE density parameters, and $\mathcal{N}$ collectively denotes all of the data nuisance parameters that need to be marginalized over. All parameters are sampled from sufficiently wide flat priors. In particular, the range for the X bins is set to be $[1 - \Delta_X, 1 + \Delta_X]$ with $\Delta_X = 4$ as the default value. Note that the value of X in the first bin is fixed by definition in Equation (1): $X_1 = X(a = 1) = 1$. The range of nearby bins is then effectively reduced by the correlations induced by the prior. In addition, the sampling procedure guarantees $H^2(a) > 0$ at all times. To test how the reconstruction and Bayesian evidence for dynamical DE change with the strength of the prior, we additionally perform reconstructions for a set of Δ_X values logarithmically spaced in the interval $\Delta_X \in [0.01, 4]$. We also run a special case with $\Delta_X = 0$, which represents the ΛCDM model, for a comparison. A modified version of CAMB[8] (Lewis et al. 2000) is used to calculate theoretical predictions.

3. Results

Panel (A) of Figure 1 compares our reconstructed $X(z)$ to the one derived from $w_{\rm DE}^{\rm eff}(z)$ reconstructed in Zhao et al. (2017) using similar data, showing them as mutually consistent. The $X(z)$ derived from $w_{\rm DE}^{\rm eff}(z)$ is strictly positive, as using the EOS implicitly assumes the positivity of the DE density that can bias the reconstruction. Separate reconstructions from individual data sets are presented in the Appendix C, showing that the H_0 and the LyαFBAO data both drag $X(z)$ toward negative values at high z. The best-fit parameters of XCDM are given in Table 1. From the values of X at various redshifts, we can see that the oscillatory features of energy density is favored by the combined data.

Figure 2 compares $H(z)$ and $D_A(z)$ derived from the reconstructed $X(z)$ to their observed values, with all quantities rescaled by their best-fit ΛCDM values. The oscillatory features in the derived $H(z)$ and $D_A(z)$ at $z \lesssim 0.7$, which are directly related to those in $X(z)$ shown in panel (A) of Figure 1, are driven by measurements of H_0, SNe and TomoBAO. The bump-and-damp feature in $H(z)$ at $z \gtrsim 0.7$ (also seen in the reconstruction performed in Poulin et al. 2018), on the other hand, is due to the LyαFBAO measurement and the integral constraint of the CMB. This can be read from the improved χ^2 listed in Table 2, namely, the XCDM model reduces the χ^2 of TomoBAO, LyαFBAO, H_0 and SNe by 4.9, 4.3, 4.1, and 4.1, respectively, meaning that it is these data sets that contribute the most to the features in X.

In Figure 1, in addition to X, we show the normalized effective DE pressure, $Y(z) \equiv P_{\rm DE}^{\rm eff}(z) / \rho_{\rm DE}^{\rm eff}(0)$[9] derived via $Y = -X + \frac{1}{3}dX/dz(1 + z)$, and the deceleration parameter, q (z). As shown in panel (B), $Y(z)$ oscillates around the ΛCDM prediction of -1, and, interestingly, DE is within $\sim 1\sigma$ of having zero pressure at $z \simeq 0.1$, 0.5, 0.9 and $z \gtrsim 3$. Panel (C) shows $q(z)$ oscillating around the prediction of the best-fit ΛCDM model (dashed–dotted line). Unlike in ΛCDM, where the acceleration starts at $z \sim 0.6$, the best fit XCDM universe would not be accelerating until $z \sim 0.45$, and would experience
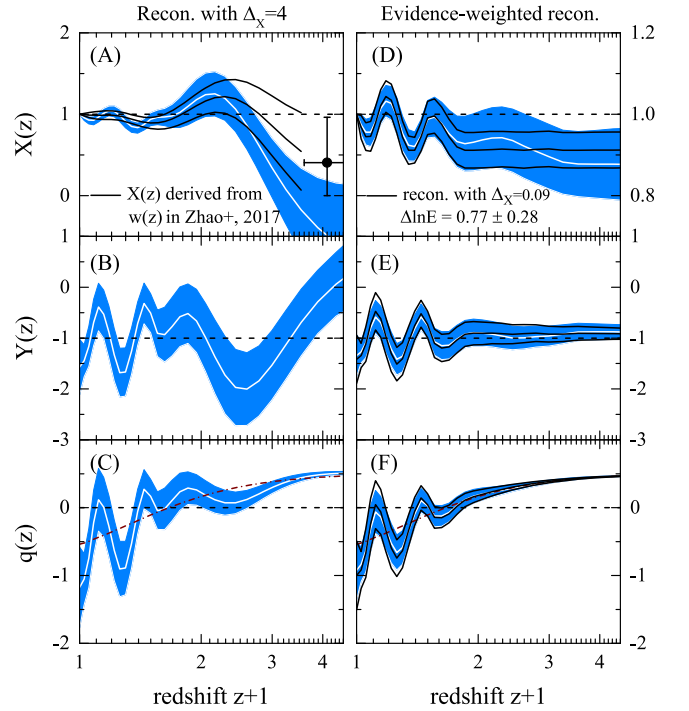

Figure 1. Panel (A): $X(z)$ (best-fit and 68% CL uncertainty) reconstructed using our standard correlated prior (blue filled band) compared to $X(z)$ derived from $w_{\rm DE}^{\rm eff}(z)$ reconstructed in Zhao et al. (2017; black curves and a data point with error bars); panel (B): the reconstructed effective DE pressure $Y(z) \equiv P_{\rm DE}^{\rm eff}(z)/\rho_{\rm DE}^{\rm eff}(0)$; panel (C): the reconstructed deceleration parameter $q(z)$. For reconstructions in panels (A)–(C), the range of variation of X in each bin is set by $\Delta_X = 4$. Panels (D)–(F): the same quantities as in panels (A)–(C) but reconstructed using $\Delta_X = 0.09$ (black solid curves), and the evidence-weighted reconstruction defined in Equation (2) (blue filled band). The wine dashed–dotted curves in panels (C) and (F) show the best-fit $q(z)$ in ΛCDM, and the dashed horizontal lines show $q = 0$ to guide the eye. The dashed horizontal lines in panels (A), (B), (D), (E) correspond to the ΛCDM model.

a short period of deceleration during $0.1 \lesssim z \lesssim 0.2$, although it is far from conclusive given the uncertainties.

The best-fit dynamical DE model reduces the χ^2 by 13.9 compared to ΛCDM, which implies that it being preferred at a 3.7σ level. However, XCDM has more degrees of freedom, and the appropriate way to assess the significance of DE dynamics is to compare the Bayesian evidences. For our "standard" prior, the Bayes factor, which is the logarithm of the ratio of the evidences, is negative, indicating no evidence for the best-fit XCDM.

To see the extent to which these conclusions depend on the choice of the prior parameters, we perform reconstructions with different prior strength and show, in Figure 3, the significance, signal-to-noise ratio (S/N), $\text{S/N} = \sqrt{|\Delta\chi^2|}$, and the evidence as functions of Δ_X (the range of variation of X in each bin). We see that, as expected, both the S/N and the evidence approach zero when the prior is very strong. Interestingly, the evidence shows a trend of climbing toward positive values as Δ_X increases, with a peak showing up at $\Delta_X \sim 0.1$, and drops below zero for $\Delta_X \gtrsim 0.4$. This motivates us to consider an evidence-weighted reconstruction, which linearly combines reconstructions with different Δ_X, weighted by the Bayesian evidence, i.e.,

$$Z_W(z) \equiv \frac{\sum_i [Z(z; \Delta_{X_i}) e^{\Delta \ln E(\Delta_{X_i})}]}{\sum_i [e^{\Delta \ln E(\Delta_{X_i})}]} \quad (2)$$
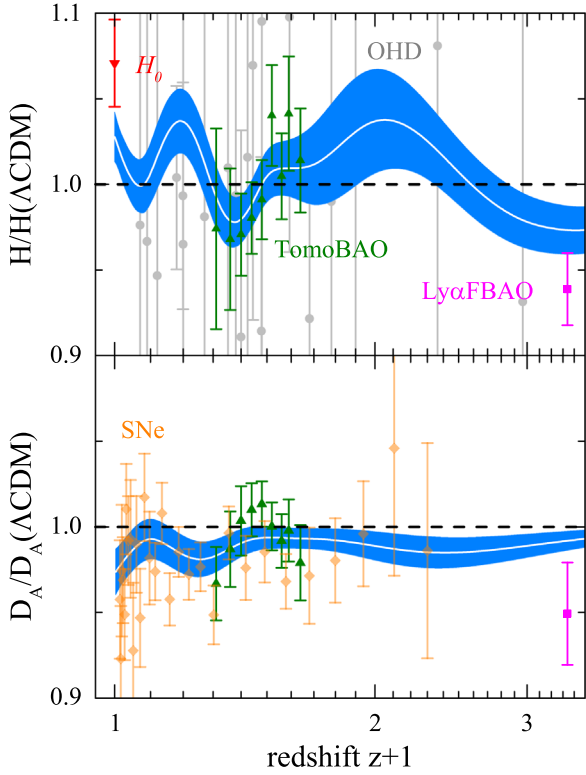
Figure 2. Top panel: $H(z)$ derived from the reconstructed $X(z)$ rescaled by that of the best fit ΛCDM model. The data points with error bars show the measurements of H as illustrated in the legend. Bottom panel: same as the top panel but for the angular diameter distance D_A.

Table 1
The Best-fit Values and the 68% CL Uncertainties of Cosmological Parameters in the ΛCDM and XCDM Models

	ΛCDM	XCDM
$\Omega_b h^2$	0.0224 ± 0.00013	0.0223 ± 0.00016
$\Omega_c h^2$	0.1189 ± 0.00087	0.1203 ± 0.00141
Θ_s	1.0412 ± 0.00029	1.0411 ± 0.00032
$X(z = 0.08)$	1	0.926 ± 0.056
$X(z = 0.18)$	1	1.042 ± 0.062
$X(z = 0.39)$	1	0.835 ± 0.068
$X(z = 1.16)$	1	1.251 ± 0.282
$X(z = 2.24)$	1	0.076 ± 0.438
Ω_M	0.302 ± 0.005	0.288 ± 0.008
H_0 [km s^{-1} Mpc^{-1}]	68.41 ± 0.387	70.30 ± 0.998

Table 2
Top Section: the Difference in χ^2 between XCDM and ΛCDM Models, $\Delta\chi^2 \equiv \chi^2_{X\text{CDM}} - \chi^2_{\Lambda\text{CDM}}$, for Individual Data Sets. Bottom Section: the Significance, $\text{S}/\text{N} \equiv \sqrt{|\Delta\chi^2|}$, and the Bayesian Evidence $\Delta \ln E$ for Reconstructions using $\Delta_X = 4$ and $\Delta_X = 0.09$, and the Evidence-weighted Reconstruction

	TomoBAO	LyαFBAO	SNe	H_0	OHD	Prior
$\Delta\chi^2$	-4.9	-4.3	-4.1	-4.1	-1.2	$+3.0$
	All data + standard correlated prior					
	$\Delta_X = 4$		$\Delta_X = 0.09$		evidence-weighted	
S/N	3.7σ		2.8σ		$(2.5 \pm 0.06)\sigma$	
$\Delta \ln E$	-5.7 ± 0.3		0.77 ± 0.28		N/A	
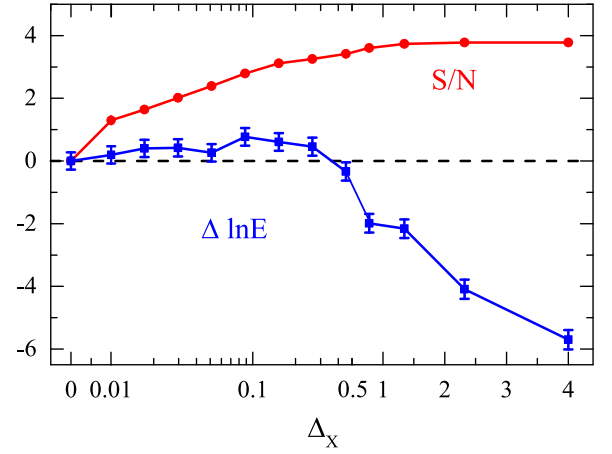
Figure 3. Bayes factor relative to that of the ΛCDM ($\Delta \ln E$) and the significance level of deviation from ΛCDM ($\text{S}/\text{N} \equiv \sqrt{|\Delta\chi^2|}$) for different values of Δ_X that set the range of variation of X in each bin.

where $Z = X, Y, q$. The evidence-weighted reconstructions are shown in panels (D)–(F) of Figure 1. They retain the key features of the best-fit XCDM shown in panels (A)–(C), but at a lesser significance. In particular, the overall significance of the deviation from ΛCDM reduces to $(2.5 \pm 0.06)\sigma$. Panels (D)–(F) show the results for $\Delta_X = 0.09$, which corresponds to the maximal Bayesian evidence $\Delta \ln E = 0.77 \pm 0.28$. We find them to be quite similar, as expected, because the linear combination in the evidence-weighted reconstruction is dominated by the component with maximal weight.

4. Conclusion and Discussions

Different levels of tension among various kinds of observations within the framework of ΛCDM necessitates the exploration of extended cosmological models beyond ΛCDM. As was shown in an earlier study (Zhao et al. 2017), dynamical DE parameterized in terms of its EOS is able to release the tension, but is not favored over ΛCDM by the Bayesian evidence.

In this Letter, we take a another route to investigating the evolution of DE; namely, we directly reconstruct the effective DE density X from data. This is advantageous over reconstructing the EOS, as X is more directly related to data, while the EOS is related to the derivative of $H(z)$. Thus, we caution against parameterizing DE in terms of its EOS as it generally biases toward positive values and smoother evolution of the DE density. This can affect the Bayesian evidence—one can obtain from the same data a positive Bayes while using $X(z)$, and a negative one when using $w_{\text{DE}}(z)$. Furthermore, X is more physically relevant in modified gravity theories, where it can be negative and change sign. Such dynamics would be forbidden for X derived from an EOS.

We find hints of DE dynamics at a significance of 3.7σ with interesting features. For example, X oscillates around the ΛCDM prediction at $z \lesssim 0.7$, and can become negative at $z \gtrsim 2.3$; DE can be pressure-less at multiple redshifts during evolution, and a short period of cosmic deceleration is allowed by current data at $0.1 \lesssim z \lesssim 0.2$. We note that these features would have been missed if the DE density was parameterized using a simple polynomial (Lemos et al. 2018). Some of these dynamical features, including the oscillations, are supported by the Bayesian evidence (the Bayesian factor is positive at about

2.8σ level for the case of $\Delta_X = 0.09$, for example), which is the first time a dynamical DE with a positive Bayesian evidence is detected. Furthermore, the evidence-weighted reconstruction prefers the dynamical DE at a $(2.5 \pm 0.06)\sigma$ significance level.

The new features of DE dynamics await scrutiny by forthcoming BAO measurements by Dark Energy Spectroscopic Instrument,[10] Euclid,[11] and Prime Focus Spectrograph.[12] Gravitational wave sources accompanied by electromagnetic counterparts will also offer accurate independent estimates of H_0 at very low redshifts (Abbott et al. 2017; Guidorzi et al. 2017; Hotokezaka et al. 2018). The methodology developed in this Letter will be useful in further studies of DE and modified gravity.

Appendix A
The Effective DE Density in General Cosmologies

In what follows, we show that in modified gravity theories the effective DE density $X(a)$, defined in Equation (1), is allowed to change sign. To see this, consider the class of generalized Brans–Dicke models described by the action (Bergmann 1968; Nordtvedt 1970; Wagoner 1970)

$$S = \int d^4x \sqrt{-g} \left[\frac{F(\phi)R}{16\pi G} - \frac{1}{2}\partial^\mu \phi \partial_\mu \phi - V(\phi) + \mathcal{L}_M \right],$$

where $\mathcal{L}_M$ is the Lagrangian of all particle and radiation fields. The modified Einstein equation in this model is

$$G_{\mu\nu} = 8\pi G F^{-1}\{T^M_{\mu\nu} + T^\phi_{\mu\nu} + \nabla_\mu \nabla_\nu F - g_{\mu\nu}\Box F\}$$
$$= 8\pi G \{T^M_{\mu\nu} + (T^{\text{eff}}_{\text{DE}})_{\mu\nu}\}, \qquad (3)$$

where, in the second line, we have defined the effective DE stress-energy by absorbing into it all of the terms on the right-hand side other than the usual matter term, i.e.,

$$(T^{\text{eff}}_{\text{DE}})_{\mu\nu} \equiv F^{-1}\{T^\phi_{\mu\nu} + \nabla_\mu \nabla_\nu F - g_{\mu\nu}\Box F + (1 - F)T^M_{\mu\nu}\}. \quad (4)$$

Then, the effective DE density is

$$\rho^{\text{eff}}_{\text{DE}} = F^{-1}\{\dot{\phi}^2/2 + V(\phi) - 3H\dot{F} + (1 - F)\rho_M\}, \qquad (5)$$

while the effective DE pressure is

$$p^{\text{eff}}_{\text{DE}} = F^{-1}\{\dot{\phi}^2/2 - V(\phi) + 2H\dot{F} + \ddot{F}\}. \qquad (6)$$

The $\mu = \nu = 0$ component of Equation (3) for a Friedmann–Robertson–Walker background metric gives the usual Friedmann equation

$$H^2 = \left(\frac{\dot{a}}{a}\right)^2 = \frac{8\pi G}{3}[\rho_M(a) + \rho^{\text{eff}}_{\text{DE}}(a)], \qquad (7)$$

which can then be recast in the form of Equation (1).

The effective DE "fluid" is, by construction, conserved,

$$\dot{\rho}^{\text{eff}}_{\text{DE}} + 3H(\rho^{\text{eff}}_{\text{DE}} + p^{\text{eff}}_{\text{DE}}) = 0, \qquad (8)$$

but its EOS,

$$w^{\text{eff}}_{\text{DE}} = \frac{\dot{\phi}^2/2 - V(\phi) + 2H\dot{F} + \ddot{F}}{\dot{\phi}^2/2 + V(\phi) - 3H\dot{F} + (1 - F)\rho_M}, \qquad (9)$$

is not always well-defined because $\rho^{\text{eff}}_{\text{DE}}$ in the denominator is allowed to change sign thanks to the new terms generated by the non-minimal coupling $F(\phi)$. In the case of quintessence, $F = 1$, the effective DE EOS is the same as the EOS of the scalar field, $w_\phi \geqslant -1$. For a general $F(\phi)$, the scalar field mediates a force between matter particles, coupling the matter fluid with DE so that they are no longer separately conserved. Thus, as articulated in Carroll et al. (2005) and Das et al. (2006), observing $w^{\text{eff}}_{\text{DE}} < -1$, or finding that $\rho^{\text{eff}}_{\text{DE}}$ changes its sign, could be a smoking gun for new interactions in the dark sector.

Appendix B
Investigating Alternative Priors and High-z Parameterizations of $X(z)$

The reconstructed evolution of $X(z)$ from the combination of all data using our "standard" prior is shown in Figure 4. To help interpret the reconstruction, we also show the 1σ uncertainties around on the 40 bins from our Gaussian prior alone. The latter are obtained by running CosmoMC and letting it converge with using just the prior and no data. The fiducial model assumed by the prior is $X(z) = 1$, and the "best fit" to the prior alone is very close, although not identical to it, as expected. One can see that at lower redshifts the data significantly improves on the prior, while at high redshifts the reduction in uncertainties is relatively small.

There are no data points probing the expansion history between $z = 2.34$, where the Lyα forest provides a BAO measurement, and the epoch of last scattering at $z \sim 1000$ probed by CMB. Thus, having several bins of $X(z)$ in that redshift range is not justified, except for the purpose of keeping the spacing between the bins uniform. To check that these "extra" bins do not affect the reconstruction of $X(z)$, we try a couple of alternative choices of parameterizing X at $z > 2.34$. Specifically, we tried replacing the last eight bins in the $a \in [0.001, 0.206]$ range ($3.85 < z < 1000$) with a single wide bin and either fixed it to $X = 1$, or let it vary independently from other bins. As shown in Figure 4, the reconstructed dynamics and the size of uncertainties at $z < 3$ remains consistent in all three cases.

Finally, in Figure 5, we show the effect of using alternative prior parameters in our reconstructions. There are two types of prior parameters: (a_c, σ_m), which set the prior covariance of the bins, and Δ_X, which sets the range of allowed values of X in each bin. In each case, we also show the 1σ uncertainties on the bins from the prior alone. The significance of the DE dynamics detection in panels (A) and (B) is 3.4σ and 2.9σ, respectively. For the stronger priors, i.e., panels (E) and (F), the reconstructions are consistent with ΛCDM.
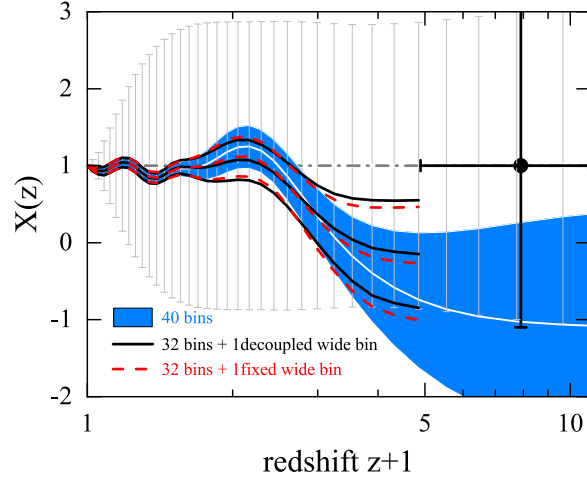

Figure 4. Reconstructed evolution of $X(z) \equiv \rho_{DE}^{eff}(z)/\rho_{DE}^{eff}(0)$ (white line with the 1σ blue band around it) obtained by fitting 40 bins uniformly spaced in $a \in [1, 0.01]$ with the help of our standard prior ($a_c = 0.06$, $\sigma_m = 0.04$). The discrete error bars show the 1σ uncertainties on the bins from the prior alone. This reconstruction is compared to two cases where the last eight bins, in the $a \in [0.001, 0.206]$ range ($3.85 < z < 1000$), are replaced with a single wide bin: this is one in which it is allowed to vary independently (red solid lines showing the best fit and the 1σ band), and one where it is fixed to 1 (green dashed lines).
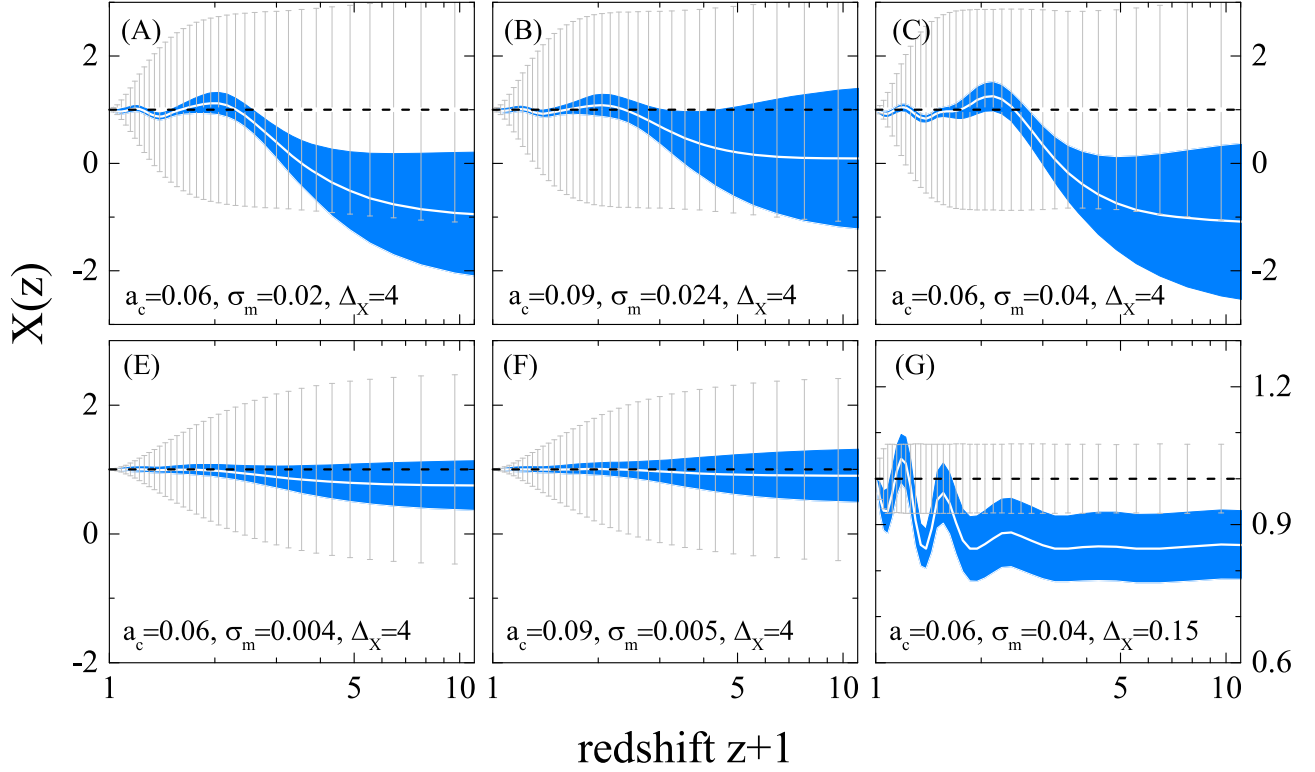

Figure 5. Comparison of the $X(z)$-reconstructions obtained using different values of the correlated prior parameters a_c and σ_m, and the range Δ_X over which X can vary in each bin. The discrete error bars show the 1σ uncertainties from the prior alone. Panel (C) is the case of our standard prior, also shown in Figure 4. Note that the vertical axis range in panel (G) differs from that in other panels.

Appendix C
The $X(z)$ Reconstructions using
Different Data Combinations

To show how each particular data set affects the reconstruction result, we reconstruct $X(z)$ from various data combinations. We first combine a collection of data sets with no reported tensions among themselves into a "Base" data set, which includes the 2015 *Planck* distance priors, JLA supernovae, and

BAO measurements from 6dFGS, MGS, and eBOSS DR14Q.[13] We then add other data sets, one at a time, to "Base" to form other data combinations, finally combining all of the data together to form the most constraining data set. The

---

[13] This Letter additionally uses the eBOSS BAO data, while excluding the galaxy power spectra, redshift space distortions, weak lensing, and CMB anisotropies, which require modeling of perturbations and were used in the EOS reconstruction (Zhao et al. 2017).
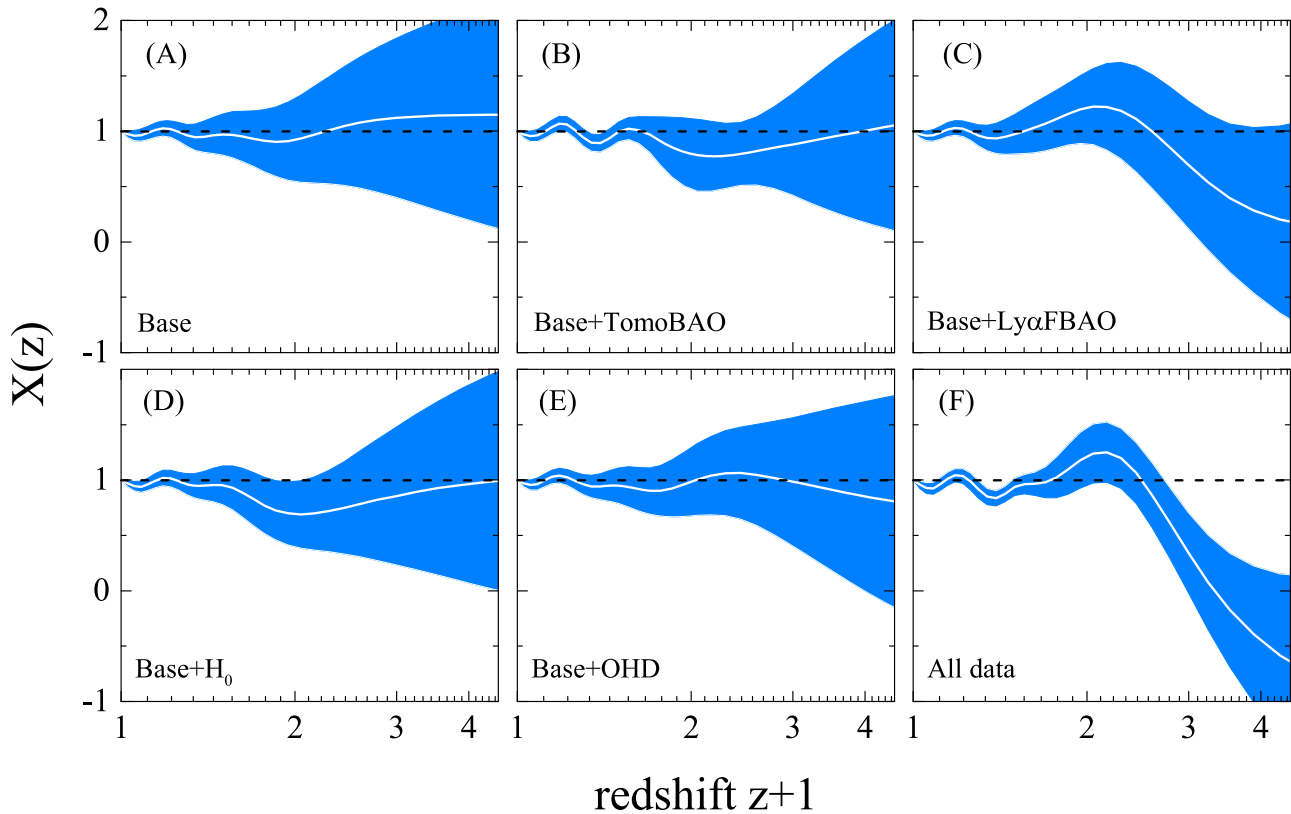
Figure 6. Panels (A)–(F): best-fit and the 68% CL uncertainty of $X(z)$ reconstructed from six different data combinations.

reconstructions of $X(z)$, i.e., the best-fit values and the 68% confidence level (CL) uncertainties for each bin, from these data sets are presented in panels (A)–(F) of Figure 6. One can see that $X(z)$ reconstructed from either Base or Base+OHD is consistent with that predicted by ΛCDM, while the reconstruction derived from the other four data combinations show different levels of dynamics in $X(z)$. For example, results derived either from Base+H_0 or Base+LyαFBAO prefer a lower $X(z)$ at higher redshifts. Specifically, Base+LyαFBAO diminishes X at $z \sim 2.3$ (it even makes X negative at $z \gtrsim 2.3$), which is due to the fact that the LyαFBAO measurement at $z \sim 2.3$ is lower than the theoretical prediction of ΛCDM at around 2.5σ (Font-Ribera et al. 2014; Delubac et al. 2015). On the other hand, Base+H_0 drags X downward at $z \sim 1$. This is because the local measurement of H_0 prefers a much greater value than that extrapolated from the best-fit ΛCDM. The most effective way to fit a higher H_0 is to increase $X(z = 0)$, but as $X(z = 0)$ is fixed to unity by definition, $X(z)$ has to be reduced at higher redshifts, namely, at $z \simeq 1$.[14] Note that, these redshift-dependent reductions of X caused by H_0 and LyαFBAO would be degenerate if one fit a constant X instead, as both data sets "pull" X in the same direction. When the tomographic BAO is added to Base, a statistically significant oscillatory feature shows up at $z \lesssim 0.6$ (see panel (B)). $X(z)$, in particular, tends to go below unity at $z \sim 0.1$ and $z \sim 0.3$ and above unity at $z \sim 0.2$. Such details would not be revealed without the high-redshift resolution BAO measurements (Wang et al. 2017; Zhao et al. 2017). The same oscillatory feature at $z \lesssim 0.6$ is present in the SNe data, and becomes more significant when all

data are combined, as shown in panel (F). The decrease in X at $z \gtrsim 1.5$ also becomes more pronounced. In addition, a new bump appears at $z \sim 1.3$ caused by the requirement to maintain a fixed distance to last scattering, set by CMB measurements, while compensating for the reduction in X at high redshifts.

ORCID iDs

Yuting Wang https://orcid.org/0000-0001-7756-8479
Gong-Bo Zhao https://orcid.org/0000-0003-4726-6714

References

Abbott, B. P., Abbott, R., Abbott, T. D., et al. 2017, Natur, 551, 85
Addison, G. E., Huang, Y., Watts, D. J., et al. 2016, ApJ, 818, 132
Ahmed, M., Dodelson, S., Greene, P. B., & Sorkin, R. 2004, PhRvD, 69, 103523
Ahmed, M., & Sorkin, R. D. 2013, PhRvD, 87, 063515
Ata, M., Baumgarten, F., Bautista, J., et al. 2018, MNRAS, 473, 4773
Bennett, C. L., Larson, D., Weiland, J. L., et al. 2013, ApJS, 208, 20
Bergmann, P. G. 1968, IJTP, 1, 25
Betoule, M., Kessler, R., Guy, J., et al. 2014, A&A, 568, A22
Beutler, F., Blake, C., Colless, M., et al. 2011, MNRAS, 416, 3017
Burgess, C. P. 2017, arXiv:1711.10592
Caldwell, R. R. 2002, PhLB, 545, 23
Caldwell, R. R., Dave, R., & Steinhardt, P. J. 1998, PhRvL, 80, 1582
Capozziello, S., Ruchika, & Sen, A. A. 2018, arXiv:1806.03943
Carroll, S. M., de Felice, A., & Trodden, M. 2005, PhRvD, 71, 023525
Carroll, S. M., Hoffman, M., & Trodden, M. 2003, PhRvD, 68, 023509
Chung, D. J. H., Everett, L. L., & Riotto, A. 2003, PhLB, 556, 61
Cline, J. M., Jeon, S., & Moore, G. D. 2004, PhRvD, 70, 043543
Conley, A., Guy, J., Sullivan, M., et al. 2011, ApJS, 192, 1
Crittenden, R. G., Pogosian, L., & Zhao, G.-B. 2009, JCAP, 12, 025
Crittenden, R. G., Zhao, G.-B., Pogosian, L., Samushia, L., & Zhang, X. 2012, JCAP, 2, 048
Damour, T., Gibbons, G. W., & Gundlach, C. 1990, PhRvL, 64, 123
Das, S., Corasaniti, P. S., & Khoury, J. 2006, PhRvD, 73, 083509
Deffayet, C., Deser, S., & Esposito-Farèse, G. 2009a, PhRvD, 80, 064015

---

[14] X is not allowed by SNe, which have a strong constraining power, to deviate from unity at $z \lesssim 1$. On the other hand, DE becomes dynamically unimportant at $z \gg 1$. Thus, to compensate for a higher H_0, X is reduced at $z \simeq 1$.

Deffayet, C., Esposito-Farèse, G., & Vikman, A. 2009b, PhRvD, 79, 084003
Deffayet, C., Gao, X., Steer, D. A., & Zahariade, G. 2011, PhRvD, 84, 064039
Delubac, T., Bautista, J. E., Busca, N. G., et al. 2015, A&A, 574, A59
Di Valentino, E., Melchiorri, A., Linder, E. V., & Silk, J. 2017a, PhRvD, 96, 023523
Di Valentino, E., Melchiorri, A., & Mena, O. 2017b, PhRvD, 96, 043503
Faraoni, V. 2003, PhRvD, 68, 063508
Font-Ribera, A., Kirkby, D., Busca, N., et al. 2014, JCAP, 5, 027
Gleyzes, J., Langlois, D., Piazza, F., & Vernizzi, F. 2015, PhRvL, 114, 211101
Guidorzi, C., Margutti, R., Brout, D., et al. 2017, ApJL, 851, L36
Handley, W. J., Hobson, M. P., & Lasenby, A. N. 2015a, MNRAS, 450, L61
Handley, W. J., Hobson, M. P., & Lasenby, A. N. 2015b, MNRAS, 453, 4384
Heymans, C., Grocutt, E., Heavens, A., et al. 2013, MNRAS, 432, 2433
Hildebrandt, H., Viola, M., Heymans, C., et al. 2017, MNRAS, 465, 1454
Hojjati, A., Pogosian, L., & Zhao, G.-B. 2011, JCAP, 8, 005
Horndeski, G. W. 1974, IJTP, 10, 363
Hotokezaka, K., Nakar, E., Gottlieb, O., et al. 2018, arXiv:1806.10596
Hu, B., Raveri, M., Frusciante, N., & Silvestri, A. 2014, PhRvD, 89, 103530
Lemos, P., Lee, E., Efstathiou, G., & Gratton, S. 2018, arXiv:1806.06781
Lewis, A., & Bridle, S. 2002, PhRvD, 66, 103511
Lewis, A., Challinor, A., & Lasenby, A. 2000, ApJ, 538, 473
Moresco, M., Pozzetti, L., Cimatti, A., et al. 2016, JCAP, 5, 014
Nordtvedt, K., Jr. 1970, ApJ, 161, 1059
Ooba, J., Ratra, B., & Sugiyama, N. 2018, arXiv:1802.05571
Peebles, P. J., & Ratra, B. 2003, RvMP, 75, 559
Perlmutter, S., Aldering, G., Goldhaber, G., et al. 1999, ApJ, 517, 565
Planck Collaboration, Ade, P. A. R., Aghanim, N., et al. 2016, A&A, 594, A13
Planck Collaboration, Aghanim, N., Akrami, Y., et al. 2018, arXiv:1807.06209
Poulin, V., Boddy, K. K., Bird, S., & Kamionkowski, M. 2018, PhRvD, 97, 123504
Ratra, B., & Peebles, P. J. E. 1988, PhRvD, 37, 3406

Raveri, M., Hu, B., Frusciante, N., & Silvestri, A. 2014, PhRvD, 90, 043513
Riess, A. G., Filippenko, A. V., Challis, P., et al. 1998, AJ, 116, 1009
Riess, A. G., Macri, L. M., Hoffmann, S. L., et al. 2016, ApJ, 826, 56
Ross, A. J., Samushia, L., Howlett, C., et al. 2015, MNRAS, 449, 835
Sahni, V., Shafieloo, A., & Starobinsky, A. A. 2014, ApJL, 793, L40
Sahni, V., & Shtanov, Y. 2003, JCAP, 11, 014
Sahni, V., & Starobinsky, A. 2006, IJMPD, 15, 2105
Scott, D. 2018, arXiv:1804.01318
Solà, J., Gómez-Valent, A., & de Cruz Pérez, J. 2017, ApJ, 836, 43
Solà Peracaula, J., de Cruz Pérez, J., & Gómez-Valent, A. 2018, MNRAS, 478, 4357
Steinhardt, P. J., Wang, L., & Zlatev, I. 1999, PhRvD, 59, 123504
Suzuki, N., Rubin, D., Lidman, C., et al. 2012, ApJ, 746, 85
Torres, D. F. 2002, PhRvD, 66, 043522
Vikman, A. 2005, PhRvD, 71, 023515
Wagoner, R. V. 1970, PhRvD, 1, 3209
Wang, Y., & Dai, M. 2016, PhRvD, 94, 083521
Wang, Y., & Tegmark, M. 2004, PhRvL, 92, 241302
Wang, Y., Zhao, G.-B., Chuang, C.-H., et al. 2017, MNRAS, 469, 3762
Wang, Y., Zhao, G.-B., Wands, D., Pogosian, L., & Crittenden, R. G. 2015, PhRvD, 92, 103005
Wetterich, C. 1995, A&A, 301, 321
Wetterich, C. 2002, SSRv, 100, 195
Yang, W., Pan, S., Di Valentino, E., et al. 2018, JCAP, 9, 019
Zehavi, I., Zheng, Z., Weinberg, D. H., et al. 2011, ApJ, 736, 59
Zhao, G.-B., Pogosian, L., Silvestri, A., & Zylberberg, J. 2009, PhRvD, 79, 083513
Zhao, G.-B., Raveri, M., Pogosian, L., et al. 2017, NatAs, 1, 627
Zhao, G.-B., Wang, Y., Saito, S., et al. 2017, MNRAS, 466, 762
Zumalacárregui, M., Bellini, E., Sawicki, I., Lesgourgues, J., & Ferreira, P. G. 2017, JCAP, 8, 019
Zwane, N., Afshordi, N., & Sorkin, R. D. 2017, arXiv:1703.06265